Generation of fuel type maps from Landsat TM images and ancillary data in Mediterranean ecosystems

David Riaño, Emilio Chuvieco, Javier Salas, Alicia Palacios-Orueta, and Aitor Bastarrika

Abstract: This paper presents methods to generate fuel type maps from remote sensing data at a spatial and temporal scale adequate for operational fire management applications. Fuel type maps account for structural characteristics of vegetation related to fire behaviour and fire propagation. A fuel type classification system adapted to the ecological characteristics of the European Mediterranean basin was adopted for this study. The Cabañeros National Park (in central Spain) area was selected for testing and validating the methods. Fuel type maps were derived from two Landsat TM satellite images and digital elevation data. Atmospheric and topographic corrections of the satellite images were performed to reduce spectral variability. A sensitivity analysis was carried out to determine the most appropriate bands for fuel type mapping. The final classification was checked by an intense field survey, the final classification accuracy being estimated at 83%. The main problem was discriminating among those fuel types that differ only in vegetation height or composition of the understory layer. The mean mapping accuracy was 15 m (0.6 pixels), and no areal discrepancy or boundary displacement with vegetation maps was apparent.

Résumé : Cet article présente des méthodes pour générer des cartes de types de combustible à partir de données de télédétection à des échelles spatiale et temporelle adéquates pour être utilisées dans la gestion opérationnelle des feux. Les cartes de types de combustible tiennent compte des caractéristiques structurales de la végétation en lien avec le comportement et la propagation du feu. Un système de classification des types de combustible adapté aux caractéristiques écologiques du bassin de la Méditérannée européenne a été adopté pour cette étude. La région du parc national Cabañeros (dans le centre de l'Espagne) a été choisie pour tester et valider les méthodes. Les cartes de types de combustible ont été produites à partir de deux images satellitaires Landstat capteur TM et de données digitales d'altitude. Les images satellitaires ont été corrigées pour tenir compte des conditions atmosphériques et topographiques afin de réduire la variabilité spectrale. Une analyse de sensibilité a été effectuée pour déterminer quelles bandes sont les plus appropriées pour cartographier les types de combustible. La classification finale a été vérifiée par un inventaire intensif sur le terrain et sa précision a été estimée à 83 %. La principale difficulté consiste à distinguer les types de combustible qui diffèrent seulement par la hauteur ou la composition de la végétation de sous-étage. La précision moyenne de la cartographie est de 15 m (0,6 pixels) et aucune divergence dans la superficie ni modification des contours ne sont apparentes comparativement aux cartes de végétation.

[Traduit par la Rédaction]

Introduction

The conjugation of human development and sustainability of natural resources is a critical issue to our present society. The role of human activity in fire occurrence is a good example of the difficult dialogue between development and conservation. Recent changes in land-use patterns in the Mediterranean basin have implied the reduction or abandonment of traditional activities, such as extensive grazing or wood harvesting, which reduced the amount of fuel available for burning. Consequently, once forest fires occur, the probability of larger events increases, since fuels are more abundant and some barriers related to land-use fragmentation are lost. The fires also increase the probability of severe soil erosion and vegetation degradation. The knowledge of fuel load and composition is, therefore, critical for improving current fire prevention and modelling programs and to alleviate the negative effects of fire on the ecosystem.

Fire behaves according to three interacting physical factors: fuel availability, weather, and terrain. Fuel conditions refer to the morphological (i.e., height, density) and physiological (i.e., moisture status) characteristics of vegetation. Weather conditions of primary importance are wind speed and direction, temperature, and relative humidity, while terrain characteristics refer to the slope and aspect, which modify fire propagation patterns.

Because the description of fuel properties is usually very complex, fire managers have described fuel classes by grouping vegetation types with similar fire behaviour char-

Received 19 November 2001. Accepted 7 March 2002. Published on the NRC Research Press Web site at http://cjfr.nrc.ca on 23 July 2002.

D. Riaño,[1] E. Chuvieco, J. Salas, A. Palacios-Orueta, and A. Bastarrika. Department of Geography, Universidad de Alcalá Colegios, 2-28801 Alcalá de Henares, Spain.

[1]Corresponding author (e-mail: david.riano@uah.es).

 DOI: 10.1139/X02-052

acteristics. More specifically, a fuel type has been defined as "an identifiable association of fuel elements of distinctive species, form, size, arrangement, and continuity that will exhibit characteristic fire behaviour under defined burning conditions" (Merrill and Alexander 1987). Vegetation species are not necessarily relevant for fire management, since the same species may present completely different fire propagation rates if their fuel load, density, vertical continuity, compactness, or surface area to volume ratio characteristics, among others, change (Deeming et al. 1978; Anderson 1982; Andrews 1986).

Two well-known fire behaviour fuel type systems are the Northern Forest Fire Laboratory (NFFL) system (Albini 1976) and the Canadian Forest Fire Behaviour Prediction (FBP) system (Lawson et al. 1985). European researchers developed a new system, in the framework of the Prometheus project, which is better adapted to fuels found in Mediterranean ecosystems (http://kentauros.rtd.algo.com.gr/promet/index.htm, Algosystems SA, Greece). These fuel types were defined for surface fire modelling, taking into account fuel height and density. The main criterion of classification is the propagation element, divided into three major groups: grass, shrubs, or ground litter. The Prometheus system is based mainly on the type and height of the propagation element, and it comprises the following seven fuel types to be identified (Fig. 1):

(1) Ground fuels (cover >50%): grass.
(2) Surface fuels (shrub cover >60%, tree cover <50%): grassland, shrubland (smaller than 0.3–0.6 m and with a high percentage of grassland), and clearcuts, where slash was not removed.
(3) Medium-height shrubs (shrub cover >60%, tree cover <50%): shrubs between 0.6 and 2.0 m, as well as young trees resulting from natural regeneration or forestation.
(4) Tall shrubs (shrub cover >60%, tree cover <50%): high shrubs (between 2.0 and 4.0 m), and regenerating trees.
(5) Tree stands (>4 m) with a clean ground surface (shrub cover <30%): the ground fuel was removed either by prescribed burning or by mechanical means. This situation may also occur in closed canopies in which the lack of sunlight inhibits the growth of surface vegetation.
(6) Tree stands (>4 m) with medium surface fuels (shrub cover >30%): the base of the canopies is well above the surface fuel layer (>0.5 m). The fuel consists essentially of small shrubs, grass, litter, and duff.
(7) Tree stands (>4 m) with heavy surface fuels (shrub cover >30%): stands with a very dense surface fuel layer and with a very small vertical gap to the canopy base (<0.5 m).

The temporal dynamism of fuel conditions traditionally requires enormous field survey efforts to keep fuel type maps current, thus constraining their operational use. Satellite remote sensing techniques provide an alternative source of fuel data, since they provide comprehensive spatial coverage and enough temporal resolution to update fuel maps in a more efficient and operational manner than traditional aerial photography (Oswald et al. 1999) or fieldwork. Additionally, satellite sensors provide digital information that can easily be connected with other spatial databases in a geographic information system (GIS) environment and imported into fire models.

Several authors have explored the use of satellite remote sensing to generate fuel type maps through digital image processing, both at regional and local scales.

Most commonly, the generation of fuel maps from remote sensing images have been based in the analysis of medium- to high-resolution sensors, such as Landsat MSS and Landsat TM data (Kourtz 1977; Burgan and Shasby 1984; Dixon et al. 1984; Yool et al. 1984; Agee and Pickford 1985; Castro and Chuvieco 1998; Vasconcelos et al. 1998; Van Wagtendonk and Root 2002). Landsat characteristics represent a good compromise between spectral and temporal resolutions and have an adequate spatial coverage for this application.

Other efforts have been concentrated in low-spatial resolution sensors, such as the U.S. National Oceanic and Atmospheric Administration Advanced Very High Resolution Radiometer images (McKinley et al. 1985; Zhu and Evans 1994). The main advantage of this sensor is the possibility of having a multitemporal database because of its high temporal coverage. This should be very useful to characterize the fuel types at regional and global scales. However, the low spatial resolution of this sensor (1 km at nadir) limits its utility to local scale. The classification accuracy of fuel-type discrimination may be rather low when the fuel beds and land-use patterns are very complex, such as those found in the Mediterranean basin.

New sensors, such as hyperspectral and radar have been also tested for this application. For instance, the Airborne Visible/Infrared Imaging Spectrometer imager (with 224 bands) has been used for the spectral characterization of fuel types (Roberts et al. 1997). While sensors of this type have great potential for mapping vegetation properties because of their high spectral resolution, they have been limited by the reduced spatial coverage they provide. New satellite hyperspectral sensors, such as Hyperion (http://eo1.gsfc.nasa.gov) and Modis (http://modis.gsfc.nasa.gov) may change this situation in the near future.

Radar data has also provided complementary information for fuel mapping, since radar is very sensitive to temporal and spatial variation of the canopy biomass (Beaudoin et al. 1994).

An estimation of canopy height would help to identify the fuel types. SPOT-HRV has been used to estimate this parameter using empirical approaches (De Wulf et al. 1990). Radar data can provide a more direct estimation (Hyyppa et al. 2000; Toutin and Amaral 2000). But accuracies of these methods do not address resolutions finer than 5 m. Upcoming satellite LIDAR (active sensors working with laser) sensors such as VCL or GLAS (Blair and Hofton 1999) will provide an accuracy of 1 m (www.geog.umd.edu/vcl/). Airborne LIDAR has already been tested, providing better results than aerial photography or airborne profiling radar (Hyyppa and Hallikainen 1996; Hyyppa et al. 2000, 2001; Lefsky et al. 2001).

Accurate fuel type maps provide information for fire managers to carry out prevention, detection, and suppression strategies, such as forest cleaning, prescribed burning, and vigilance tower locations.

Objectives

The goal of this paper is to evaluate the potential of Landsat TM bands in combination with ancillary data to discrimi-

Fig. 1. Scheme used to identify the fuel types.

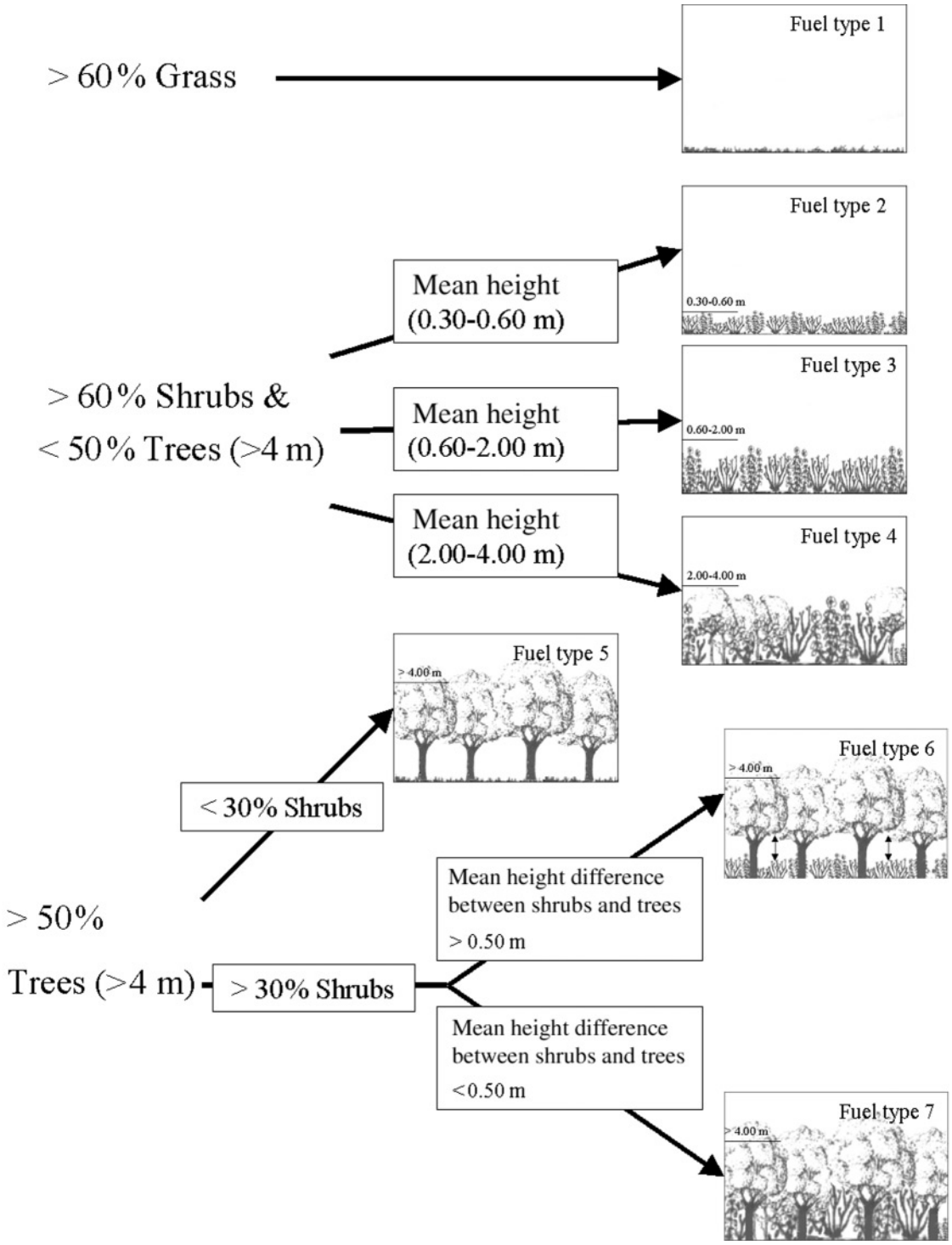

nate Mediterranean fuel types as defined in the Prometheus project, and to develop a robust methodology to operatively obtain fuel-type maps for fire prevention and fire-behaviour modelling.

Topographic variables and texture bands have been successfully added to the original bands for digital classification of fuel types (Chuvieco and Salas 1996). Therefore, the ability to improve classification accuracy using these variables was also tested. The mapping accuracy was also assessed.

Study area

Cabañeros National Park is located about 200 km south of Madrid (Fig. 2) on the western area of Spain's southern plateau, and occupies an area of around 41 000 ha.

The Park forms part of the southern limit of the Toledo Mountains, which comprise a series of small mountain ranges or "sierras" with a NW–SE direction. Elevations vary from around 900–1400 m along the sierra ridges, to about

Fig. 2. Study area. Spring image (May 5, 1998).

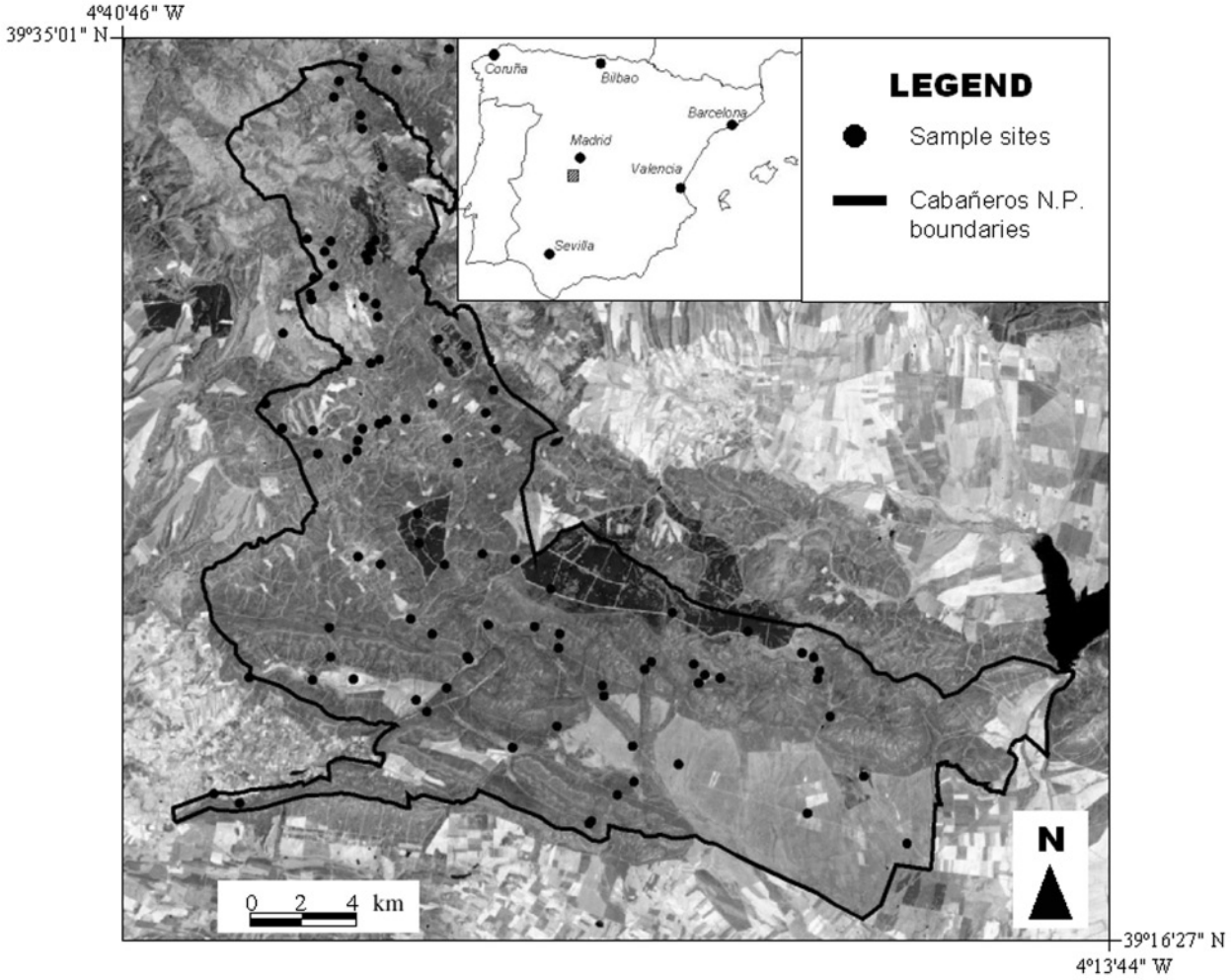

500–700 m at the foot of the valleys. The Park's main features consist of a series of Paleozoic sierras intermingled with Plioquaternary conglomerates or "rañas" which are flat wide plains formed of eroded quartzite pebbles from the surrounding sierras. Predominant lithology includes quartzites, sandstone, slates, and conglomerates. Because of their different resistance to erosion, these rocks have formed an uneven Appalachian relief in which the hard rocks like sandstone and quartzites tend to remain on the higher areas, whereas the softer ones (slate and schists) form the valley bottoms.

The climate in Cabañeros is a clear example of the characteristic warm temperate inland Mediterranean type in Spain (mean temperature around 13–16°C), where cold rainy winters, short wet springs and autumns, and hot dry summers, best describe the general climatic characteristics, which can, however, vary locally in the mountainous areas. Thus, on northwest-facing slopes, temperatures may drop from 0.4 to 0.6°C/100 m depending on the season, and yearly rainfalls range from 500 to 850 mm/year. Summer weather produces by far the greatest fire danger conditions, because the months of June, July, and August get only 7–12% of the annual rainfall, and the mean temperatures range from 23 to 25°C.

Cabañeros is one of the best examples of Iberian–Mediterranean forest. The Park's main forest species, in order of importance and abundance, are holm oak (*Quercus ilex*), cork oak (*Quercus suber*), and gall oak (*Quercus faginea*). The distribution and density of trees vary greatly according to terrain, temperature, and humidity. In the flat low "rañas" we find parklike woodlands or "dehesa", that is, large grazing pastures with scattered old holm oaks. This area has traditionally been used for extensive grazing or cultivation and, therefore, is cleared of shrubs, leaving only tall graminea grass species.

In the steeper, more mountainous areas, oakwoods with *Q. faginea* and *Quercus pyrenaica* are found in colder, damper climates at the mesomediterranean vegetation level. *Quercus pyrenaica* and *Sorbus torminalis* usually grow together at high altitudes (1000 m and over), or in valleys with deep soil and a high water table. *Quercus ilex* tends to grow in drier areas together with *Q. suber.* Degraded areas are dominated by heliophilae species, mainly rock roses (*Cistus ladanifer, Cistus populifolius*) and heather (*Erica australis, Erica umbellata,* and *Erica arborea*). Generally, these trees and shrubs species are very flammable, especially during the summer (Vélez 2000).

Methodology

The main steps in the mapping process were the identifi-

Fig. 3. Fuel type mapping methodology.

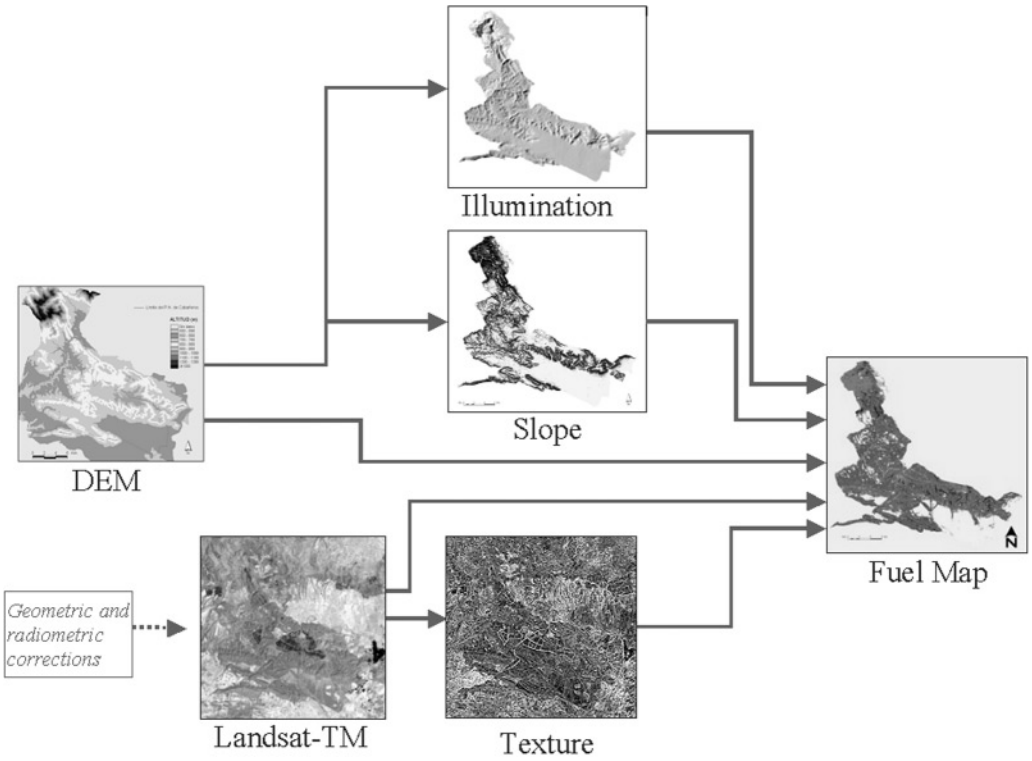

cation of fuel types in Cabañeros National Park according to the Prometheus system and the discrimination of these classes using multitemporal Landsat TM images and ancillary data (Fig. 3).

Identification of fuel types

A total of 102 land plots were located and sampled in the field, exhaustively covering the study area (Fig. 2). These plots were located in homogenous fuel areas using a global positioning system (GPS) differential receiver. Main vegetation species, density, coverage, height, slope, aspect, location, and date were noted. Stratified sampling was used to select an equal number of samples per fuel type according to their abundance, based on previous knowledge of the terrain. The scheme shown in Fig. 1 was used to identify the Prometheus fuel types. This ground-truth information was used to train the classification algorithm and assess the results.

The plots accounted for different exposures, slopes, density, and species. A total of nine pixels per plot were selected for the classification accuracy assessment, whereas the surrounding area with the same fuel type was used for the training. Therefore, no training pixels were used for the classification accuracy assessment.

Generation of digital elevation model data

A digital elevation model (DEM) of the area was generated by spatial interpolation of digitized contour lines from a 1 : 50 000 scale map (contours every 20 m), using the distance transform algorithm (Rosenfeld and Pfaltz 1968). Since all the fieldwork was carried out in the National Park, elevation data was only produced within the Park and the surrounding areas (Fig. 4). The DEM was used to generate the slope and illumination map. The slope computed at each pixel is the plane formed by the vector connecting the left and right neighbours versus the vector connecting the upper and lower neighbours of the pixel. The illumination of each pixel was computed considering the solar zenith and azimuth angle when each Landsat TM image was acquired, as well as the slope and aspect of each pixel.

Selection and processing of satellite images

Landsat TM images were selected for this project because of the good spatial and spectral resolution provided by this sensor. As is well known, Landsat TM data include spectral information from visible (three bands in the blue, green, and red wavelengths), near infrared (0.7–0.9 μm), and shortwave infrared bands (two bands at 1.6 and 2 μm) with a spatial resolution of 30 × 30 m and a thermal infrared (10–12 μm) band with a 120 × 120 m resolution.

A spring image (May 5, 1998) and a summer image (July 24, 1998) were chosen for this project. They presented seasonal differences that account for phenological changes in the vegetation. The images were cloud free and had good illumination (large sun elevation angle), which minimized the topographic distortion.

The spring image was georeferenced using a set of 40 ground control points extracted from 1 : 50 000 scale maps. The multitemporal matching of the summer scene was assured by finding common points to the georeferenced spring image. During the geometric correction, the pixel size was changed from the original 30 × 30 to 25 × 25 m to improve the integration of the image with other data sources. For resampling, the bilinear interpolation algorithm was selected, since the original pixel size was changed.

Bilinear interpolation was used to keep better the linear structures (road, paths) of the image for an easier location

Fig. 4. Digital elevation model of the Cabañeros National Park.

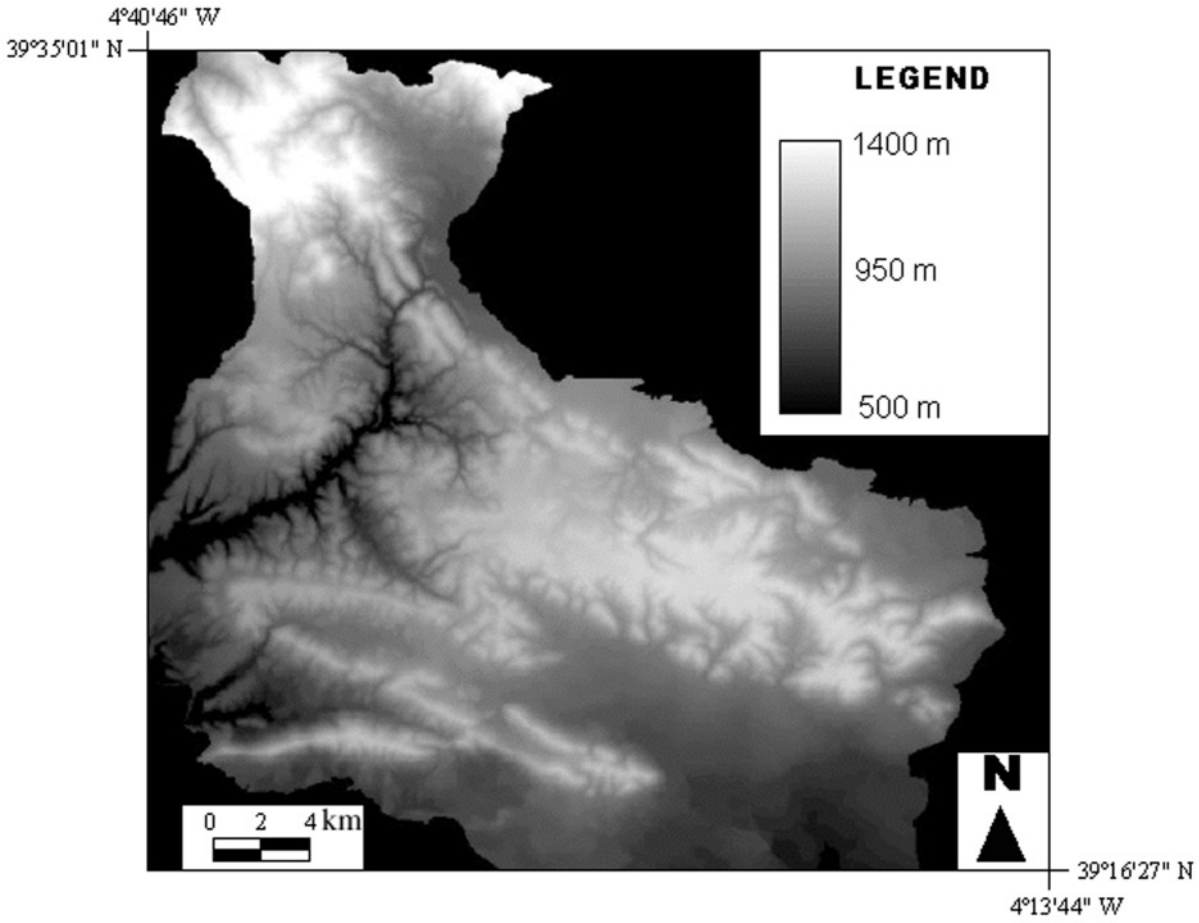

for field sampling. Some authors have proven that resampling of spectral data does not produce a reduction in the classification accuracy (Dikshit and Roy 1996).

For reducing external effects on vegetation reflectance, an atmospheric correction was applied, assuming a flat surface and lambertian reflectivity. The technique used was the default transmittance method proposed by Chavez (1996), which recommends extrapolation of the downwelling transmittance from other images. Values for bands TM1–TM4 were taken from Chavez (1996), but since the correction was proposed for neither TM5 nor TM7, transmittance values were taken from Gilabert et al. (1994) for these bands.

After performing atmospheric correction, reflectance patterns found in the images followed the most accepted criteria for assessment (PCI 1999): (*i*) the vegetation should have a reflectance peak in the green; (*ii*) water reflectance should be 0–1% for near (NIR) and short-wave infrared (SWIR); and (*iii*) bare soil reflectance increases with wavelength (steeper slope after correction, mainly for visible (VIS) bands).

Topographic correction was performed to alleviate the effects of topography on surface reflectance, namely the shadowing and change in the sun incidence angle. A non-Lambertian surface was assumed. Illumination images from both image dates were generated considering sun zenith and azimuth angles, as well as slope and aspect. Homogenization of shaded and illuminated slopes was based on the C-correction method proposed by Meyer et al. (1993). This method applies different weights to each spectral band, based on a regression between the illumination image and the calibrated reflectance for each TM band (Fig. 5).

The topographic correction was verified not only visually but also by analyzing the spectral variability before and after the correction of the 19 spectral classes that will be used in the classification process. If the correction were adequate, it would reduce the internal variability of spectral classes located on different topographic positions, since it would imply a homogenization of illumination conditions. As a matter of fact, after the topographic correction, a reduction in variability (standard deviation) of the reflectance was observed within each spectral class (Table 1), except for some TM bands of nonfuel classes and fuel types 1 and 2. Therefore, there was a homogenization of illumination conditions, at least for the fuel types that are more difficult to classify, such as medium-high shrubs and trees.

With respect to the calibration of the thermal band (TM6), surface temperatures were computed after inverting Plank's equation, using a mean value of emissivity for vegetation equal to 0.985 (Wukelic et al. 1989). This band was also resampled to 25 × 25 m.

Digital classification

Supervised classification techniques were applied to generate the fuel types using the maximum-likelihood algo-

Fig. 5. Window of the original image (left) and topographically corrected image (right). Summer image (July 24, 1998). Solid arrows show examples of places where topographic correction was effective.

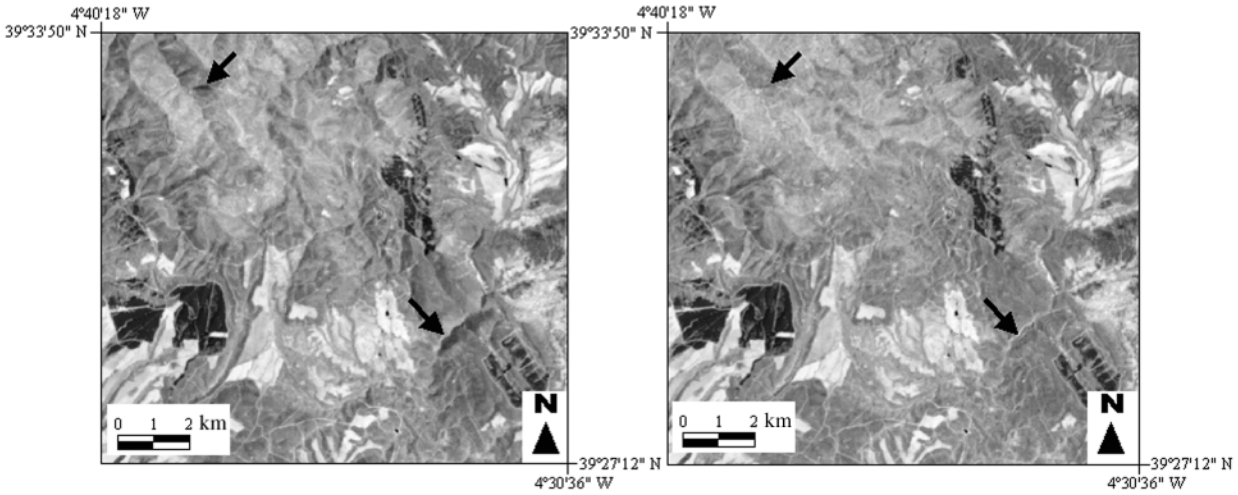

Table 1. Standard deviation reduction, in percent reflectance, after topographic correction within each spectral class for summer image (July 24, 1998).

Class	Description	TM1	TM2	TM3	TM4	TM5	TM7
1	Stony ground	0.01*	–0.05	–0.07	–0.22	0.13*	0.13*
2	Bare soil	0.01*	–0.01	–0.01	0.01*	0.07*	0.06*
3	Water	0.00	0.00	0.00	0.00	0.00	0.00
4	Fuel type 1, crop	–0.02	0.00	–0.03	–0.04	0.03*	0.13*
5	Fuel type 1, pasture	0.00	0.02*	0.01*	0.06*	0.07*	0.04*
6	Fuel type 1, dehesa	0.02*	0.07*	0.01*	0.03*	0.08*	0.00
7	Fuel type 2, *E. australis* and *C. ladanifer*	0.03*	0.03*	0.06*	0.05*	0.18*	0.12*
8	Fuel type 2, *C. ladanifer* on slates	–0.04	–0.05	–0.01	0.09*	0.06*	0.02*
9	Fuel type 3, *A. unedo* and *C. ladanifer* after fire	–0.02	–0.04	–0.03	–0.02	–0.09	–0.04
10	Fuel type 3, *C. ladanifer*, *E. australis*, and *A. unedo*	–0.05	–0.08	–0.10	–0.01	–0.36	–0.26
11	Fuel type 4, *C. ladanifer*, *E. australis*, and *A. unedo*	–0.04	–0.05	–0.04	–0.15	–0.14	–0.07
12	Fuel type 4, *Q. pyrenaica*	–0.04	–0.10	–0.11	–0.13	–0.48	–0.29
13	Fuel type 5, *P. pinaster*	0.00	0.00	–0.01	–0.11	–0.07	–0.02
14	Fuel type 5, *Q. suber* and *Q. ilex*	0.02*	0.02*	0.06*	–0.06	–0.03	0.01*
15	Fuel type 5, *Q. pyrenaica* and *Q. ilex*	–0.01	–0.04	–0.02	–0.31	–0.16	–0.08
16	Fuel type 6, *P. pinaster*	–0.01	–0.02	–0.02	–0.19	–0.10	–0.04
17	Fuel type 6, *Q. pyrenaica* and *Q. ilex*	–0.01	0.00	–0.01	–0.16	–0.12	0.00
18	Fuel type 7, mixed forest	–0.07	–0.09	–0.10	–0.23	–0.37	–0.23
19	Fuel type 7, *Q. pyrenaica*	0.00	–0.05	–0.04	–0.27	–0.36	–0.11

*No reduction observed.

rithm. Variables included in the classifications were spectral vegetation indices, endmembers, and spatial texture. Target spectral classes were defined, and the classification algorithm was applied to assign each pixel to one of the defined classes.

Generation of variables

The following variables were tested in the classification process: (*i*) TM1 to TM5 and TM7, after atmospheric and topographic correction; (*ii*) TM6 converted into surface temperature; (*iii*) elevation and derived variables (slope and illumination); (*iv*) spectral vegetation indices; (*v*) green vegetation, nonphotosynthetic vegetation and shadow endmembers; (*vi*) spatial texture (homogeneity and contrast) from the co-occurrence matrix.

Spectral vegetation indices emphasize vegetation characteristics. The vegetation indices used were the normalized difference vegetation index (NDVI) (Rouse et al. 1974), $NDII_5$ (Hunt and Rock 1989), and $NDII_7$ (the latter two with a similar formulation as the NDVI but changing the red channel by the 1.6 and 2 μm SWIR bands, respectively).

Spectral mixture analysis generates endmember bands, which are defined as the proportion of each pixel covered by a basic spectral class (Shimabukuro and Smith 1991). In this case, the endmembers chosen were shadow, green vegetation, and nonphotosynthetic vegetation. Each pixel is considered to be a linear combination of those three components,

Fig. 6. Texture image of the Cabañeros National Park computed with the standard deviation (SD) method (in percent reflectance). Spring image (May 5, 1998).

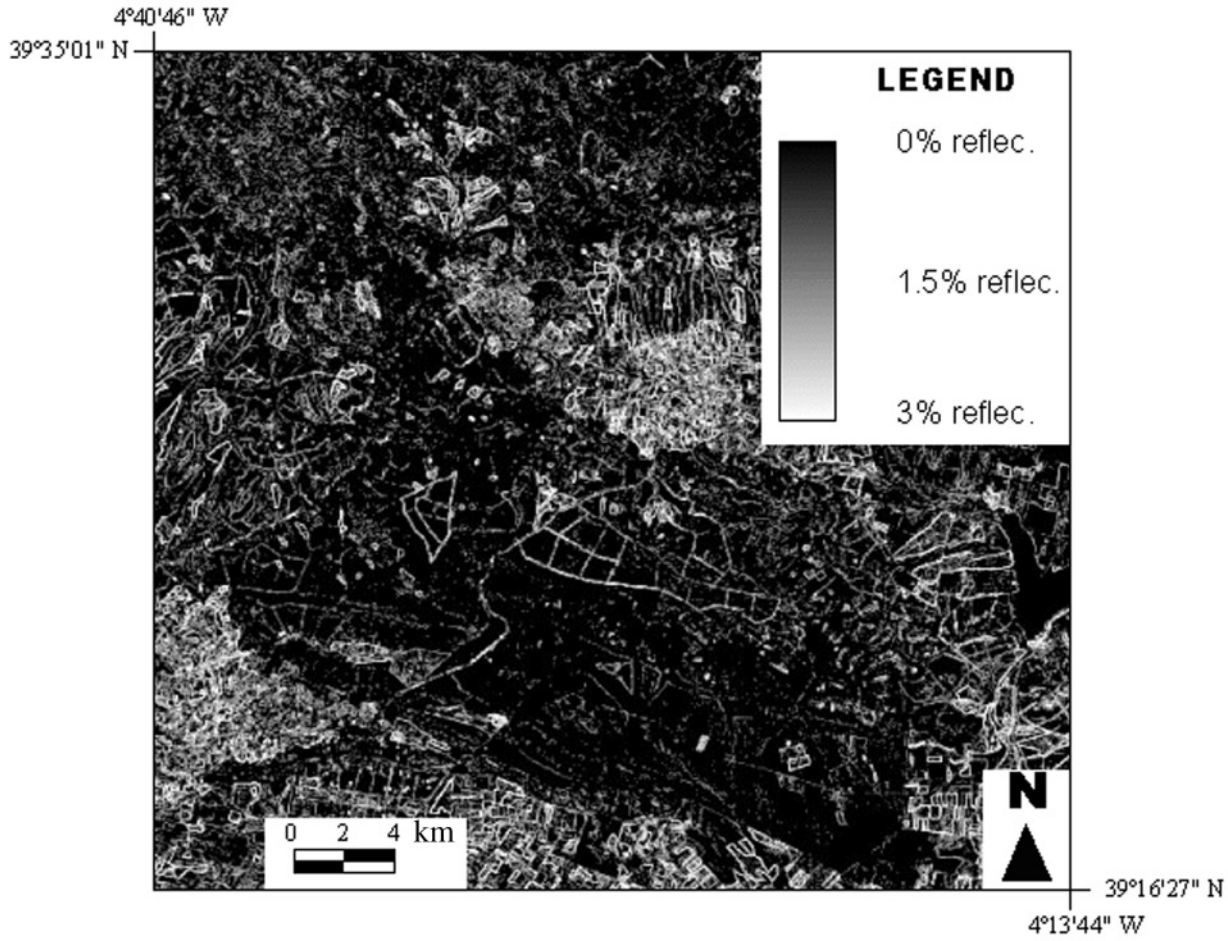

and it is assumed that the sum is equal to one and that no negative values are allowed.

Several authors have included textural measurements in the discrimination of fuel types (Cosentino et al. 1981; Yool et al. 1984). For this project, textural measurements were computed from the 3 × 3 pixel moving window co-occurrence matrix, based on a square matrix that includes the relative frequency of each pair combination of contiguous pixels (Haralick et al. 1973). Using this matrix, a measurement of the homogeneity and contrast was computed for each pixel in the TM3 band. Additionally, a measure of the occurrence matrix, such as the local standard deviation (SD) in the same 3 × 3 pixel moving window, was calculated (Fig. 6). As shrub height and density increases, roughness decreases, because the amount of bare soil and (or) dead fuels observed by the satellite also decreases. When the shrubs are mixed with trees (fuel type 7) roughness decreases, because shrubs again cover the bare soil and (or) dead fuels.

Training

Classification techniques rely on identifying the spectral classes present on the image. Although fuel types are based mainly on height and density, spectral response can be very different, e.g., pine forest and oak forest. Grouping them inside the same spectral class can give rise to classes with high spectral variability. When the spectral groups do not correspond to thematic groups, the user needs to merge or split them, with the former being the simplest process. For this project, a set of 19 relatively homogenous spectral classes (Table 1) were defined for training, since it was found that some fuel types present very diverse spectral behaviours and, therefore, should be considered independently first, then merged at the end of the process.

Assignment

Supervised and unsupervised digital classifications have been widely used. New classifiers, e.g., neural networks, have been also tested for fuel-type mapping (Vasconcelos et al. 1998). In this work, each pixel was assigned to the class to which it had the highest probability of belonging, according to the maximum likelihood algorithm (Swain and Davis 1978).

Assessment

The classification accuracy measured in previous fuel type mapping studies ranged widely (65–85%) (Agee and Pickford 1985; Vasconcelos et al. 1998) according to the fuel types considered and the verification methods used, such as field data or aerial photographs (Kourtz 1977; Burgan and Shasby 1984; Dixon et al. 1984; Yool et al.

1984; Agee and Pickford 1985; Castro and Chuvieco 1998; Vasconcelos et al. 1998). In this work the classification accuracy assessment was based on the fieldwork previously mentioned. A total of 9 pixels were chosen for each of the 102 land plots sampled in the field. The confusion matrix (Congalton 1991), relating the referenced and classified data, was used to identify the main sources of error and to numerically validate the accuracy of each classification trial.

Literature consulted on vegetation mapping using optical remote sensing data focuses mainly on classification accuracy. This concept implies the assessment on the level of agreement between classified and ground-observed categories (Congalton 1991; Fenstermaker 1994; Congalton and Green 1999; Khorram 1999). Most authors consider that mapping accuracy (the degree of geometric adjustment between classified and real boundaries) is assessed by measuring the mean root mean square of geometric correction (Congalton and Green 1999). If the images are well georeferenced there should not be areal discrepancy or boundary displacement errors in the output map. Coordinates from 40 ground-control points were taken in each image and compared with a topographic map (scale 1 : 50 000) to measure the mapping accuracy. These points were independent from the geometric correction model. Furthermore, a vegetation map independently generated from the fuel type map was used to reinforce mapping accuracy assessment. This vegetation map was produced by National Park personnel based on photointerpretation of aerial photography (1 : 10 000) and extensive fieldwork.

Results

Transformed divergence (Kumar and Silva 1977) between pairs of classes was calculated to measure the statistical separability of training statistics (Table 2). A value of 100% indicates excellent separability; 95–99.9%, good; and values under 95%, poor. Separabilities were poor for classes 10 and 17. The worst separabilities were for fuel types 5, composed of *Q. pyrenaica* and *Q. ilex* (class 15) and fuel type 6, composed of the same species (class 17). There were also poor separabilities between fuel type 3 (class 10) and fuel types 2 (class 7) and 4 (class 12).

Table 3 ranks the discrimination ability of each variable according to transformed divergence (Kumar and Silva 1977). TM7 information does not significantly help in separating target classes, so it was removed from the classification process. Synthetic bands (vegetation indices and endmembers) were not included in this analysis, because their information, which is already included in the original spectral bands, would produce a change in the ranking of the original TM bands (see the improvement in global classification accuracy assessment after adding different layers).

Confusion diagrams were also built with the mean and standard deviation of each class to illustrate the potential overlapping between classes. Figure 7 shows an example of this confusion diagrams for TM 5 band reflectance. According to the figure, this band would be very useful to distinguish classes 13 and 16 from the rest of vegetated areas.

After maximum likelihood classification, the 19 spectral classes were reclassified into 7 target fuel type classes. Additionally, another nonfuel class was extracted, to represent

Table 2. Transform divergence for every spectral class: stony ground (S), bare soil (B), water (W), and the fuel types (FT).

	S	B	W	FT1			FT2		FT3		FT4		FT5			FT6		FT7
	1	2	3	4	5	6	7	8	9	10	11	12	13	14	15	16	17	18
2	100																	
3	100	100																
4	100	100	100															
5	100	100	100	98.1														
6	100	100	100	100	100													
7	100	100	100	100	100	100												
8	100	100	100	100	100	100	100											
9	100	100	100	100	100	100	100	100										
10	100	100	100	100	100	100	90.7*	100	100									
11	100	100	100	100	100	100	100	100	100	100								
12	100	100	100	100	100	100	97.9	100	100	82.4*	100							
13	100	100	100	100	100	100	100	100	100	100	100	100						
14	100	100	100	100	100	100	100	100	100	100	100	100	100					
15	100	100	100	100	100	100	99.8	100	100	95.1	100	98.8	100	100				
16	100	100	100	100	100	100	100	100	100	99.5	100	100	98.9	100	100			
17	100	100	100	100	100	100	99.8	100	100	84.0*	100	90.8*	100	100	71.0*	99.4		
18	100	100	100	100	100	100	100	100	100	100	100	100	100	100	100	100	100	
19	100	100	100	100	100	100	100	100	100	100	95.9	100	100	100	100	100	100	100

*Poor separability.

Fig. 7. Mean and standard deviation of each spectral class for TM5. Spring image (May 5, 1998).

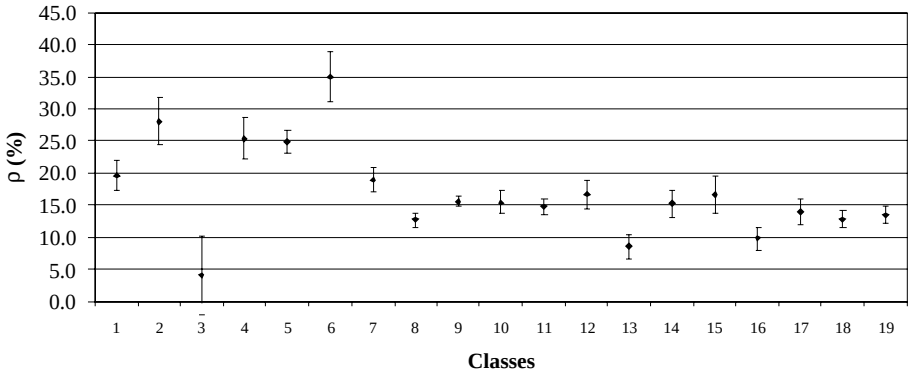

Table 3. Bands ordered in terms of separability for the spectral classes (only one date included).

Separability	Layer
High	Illumination
	Elevation
	TM5
	TM3
	Texture TM3
	TM4
	Slope
	TM6
	Texture TM5
	TM2
	Homogeneity (TM3)
	TM1
	Homogeneity (TM5)
Low	TM7

Table 4. Improvement in global accuracy after adding to the classification the layers shown in the table.

Layers	Improvement in global accuracy (%)
TM6	2.07
DEM	5.55
Slope	3.92
Illumination	1.63
Homogeneity (TM3)	2.29
Homogeneity (TM5)	0.98
DT (TM3)	0.76
DT (TM5)	0.55
GV	–0.11
NPV	–2.29
Shadow	–4.03
NDVI	0.11
NDII5	0.19
NDII7	0.09

stony ground, bare soil, and water. A 3 × 3 modal filter was used to smooth the results of the classification (Fig. 8).

Table 4 shows the improvement in global classification accuracy after adding different layers to the Landsat bands TM1–TM5. As can be seen, topographic variables, the thermal band, and textures improve the classification. However, synthetic bands (endmembers and vegetation indices) do not significantly improve the results.

The global classification accuracy (Table 5) using TM1–TM5 was 57.8%. After taking into account the spring and summer images, the classification accuracy increased to 67.3%. This implies a significant improvement, at the 95% confidence level, versus the analysis using TM1–TM5. The confidence intervals do not overlap. The results improve to 79.4% classification accuracy after adding the topographic variables, a significant difference versus previous analysis at the 95% confidence level. Finally, including textures and the thermal band increased the classification accuracy to 82.8%, which is not a significant difference versus previous case, at the 95% confidence level. The Kappa index, a widely used statistic in classification accuracy assessment (Congalton 1991), makes it possible to compare results from different classification methods. In this case the best result, after including the TM1–TM5, the topographic variables, textures and thermal band, provides a Kappa index of 0.793, which indicates that the classification was 79.3% better than expected by chance.

Table 6 presents the confusion matrix after the classification stage. The main problems were distinguishing fuel type 3 (medium height shrub) from 2 (low shrub) and 4 (tall shrub), according to the best classification produced (using TM1–TM6 from both dates, plus elevation, slope, illumination, and texture layers). Discrimination between fuel types 5 and 6 (mixtures on shrubs and trees with different cover density) was an additional problem.

The mapping accuracy was estimated by the mean displacement of 40 independent ground-control points located in both images. Estimated error was 15 m (0.6 pixels). Overlapping the classified image and boundaries of the photointerpretation map for selected categories confirmed the appropriate mapping accuracy of the final fuel type map (Figs. 9 and 10).

Discussion

The global classification accuracy of the fuel type map significantly increased after including two seasonal Landsat TM images, because the phenological state of the fuel types

Fig. 8. Fuel type map.

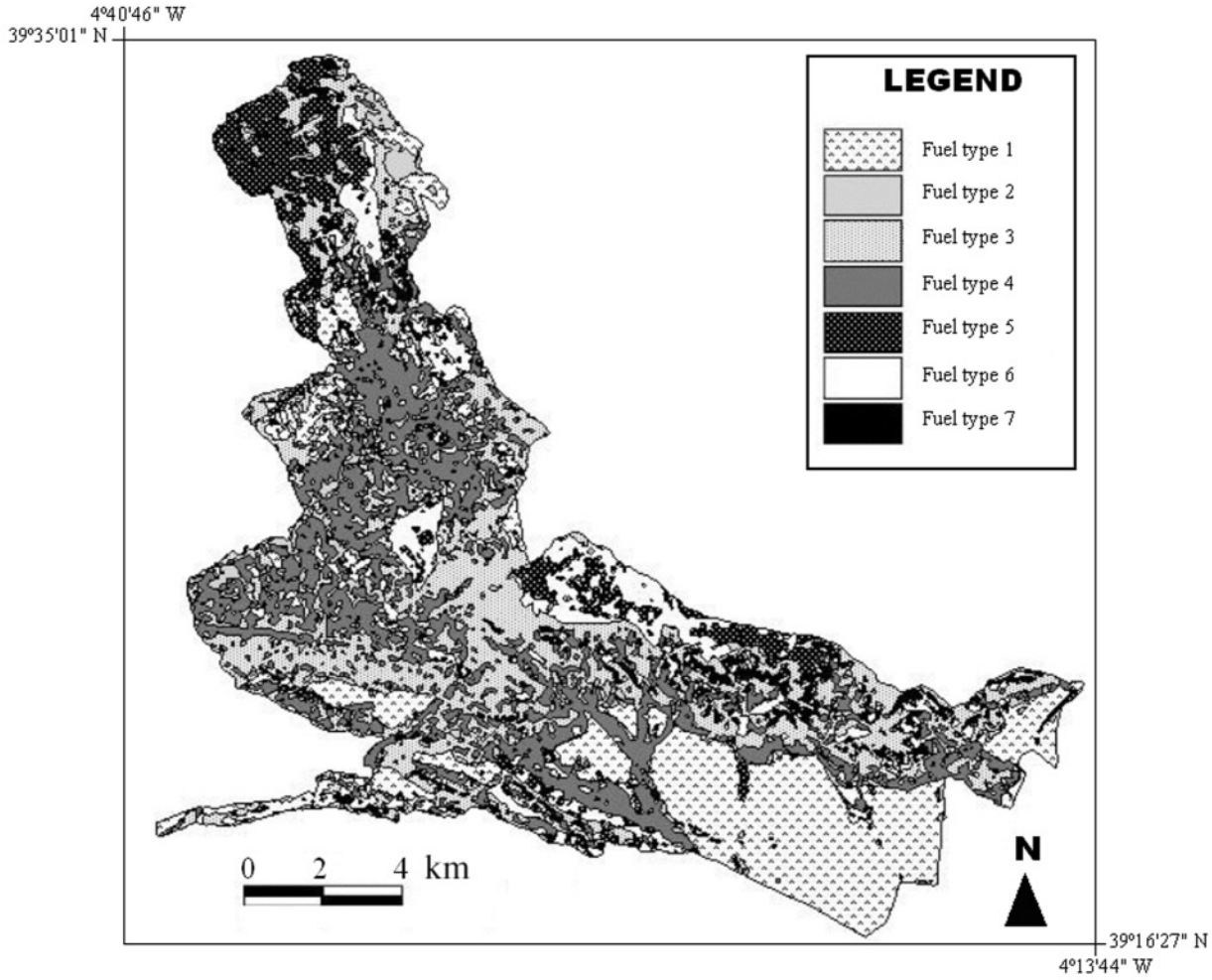

was taken into account. A deciduous forest in spring does not cover the entire ground surface so the presence of understory vegetation can be distinguished. Therefore, a fuel type 5 could be discriminated from 6, even though both of them were composed of deciduous forest.

Synthetic bands (endmembers and vegetation indices) are commonly used to enhance certain properties of the vegetation. However, according to our results they did not improve fuel type mapping (Table 4), since the original Landsat bands already contain the most significant information. Using both the original and synthetic bands did not improve the classification process. Equally, TM7 does not help in separating the fuel types according to Table 3, because the information to distinguish fuel types is already included in other bands (mainly TM5). Therefore, it was not taken into account in the classification process.

Topographic layers such as elevation, slope, and illumination were important in classifying the fuel types (Table 4), because environments and, therefore, fuel types differ according to altitude, slope, and aspect. Fuel types that had similar spectral response, e.g., fuel type 5 composed of pine forest and fuel type 6 composed of pine forest with understory vegetation, could be better separated using these ancillary variables.

Spatial texture retrieves differences between fuel types in terms of vegetation density, and indirectly, vegetation height. However, some misclassifications (Table 6), which were already predictable through a priori analysis of separability, remained (Table 2). There were problems in distinguishing fuel type 3 from fuel types 2 and 4, which differed primarily in vegetation height. Fuel type 2 (<0.6 m) versus 4 (>2.0 m) error was smaller, since the vegetation height difference is larger. There were also errors between fuel types 5 and 6 because of difficulty in identifying the presence–absence of understory. On the other hand, fuel type 7 provided better classification accuracy, even though there is understory, because of more widely spaced trees, which provides more light for the understory to grow and, consequently, a different spectral signal.

Additionally, it was proven that map accuracy was high. Figures 9 and 10 show how the boundaries extracted from the vegetation map matches those derived from the classified fuel type map. In the case of Fig. 9, it is shown the agreement between pine forest extracted from the vegetation map and the fuel type classes 5 and 6 (corresponding both to forested stands). Figure 10 illustrates the degree of correspondence between boundaries of shrub lands, which corresponds mainly to shrub fuel types 3 and 4.

Table 5. Global accuracy and kappa (κ) statistics for different digital classifications, with the confidence interval (CI).

	Global accuracy (%)	95% CI	κ
TM1–TM5 bands	57.8	54.6–61.0	0.508
TM1–TM5 bands (multitemporal)	67.3	64.3–70.4	0.613
Multitemporal + DEM + slope + illumination	79.4	76.8–82.0	0.754
Multitemporal + DEM + slope + illumination + TM6 + texture	82.8	80.3–85.2	0.793

Table 6. Confusion matrix using TM1–TM6 from both images, DEM, slope, illumination and texture layers.

	Reference fuel type										
Classified fuel type	1	2	3	4	5	6	7	No fuel	Total	User's accuracy (%)	Error of commission (%)
1	134	0	0	2	3	0	0	1	140	95.7	4.3
2	0	34	14	2	1	0	0	0	51	66.7	33.3
3	0	5	186	32	3	2	3	0	231	80.5	19.5
4	0	1	19	105	0	5	2	0	132	79.5	20.5
5	1	5	6	1	114	10	1	0	138	82.6	17.4
6	0	0	9	9	14	127	5	0	164	77.4	22.6
7	0	0	0	2	0	0	43	0	45	95.6	4.4
No fuel	0	0	0	0	0	0	0	17	17	100.0	0.0
Total	135	45	234	153	135	144	54	18	918		
Producer's accuracy (%)	99.3	75.6	79.5	68.6	84.4	88.2	79.6	94.4			
Error of omission (%)	0.7	24.4	20.5	31.4	15.6	11.8	20.4	5.6			

Fig. 9. The boundary of pine stands (*Pinus pinaster*) from the photointerpreted map are superimposed on the fuel type map produced by digital classification.

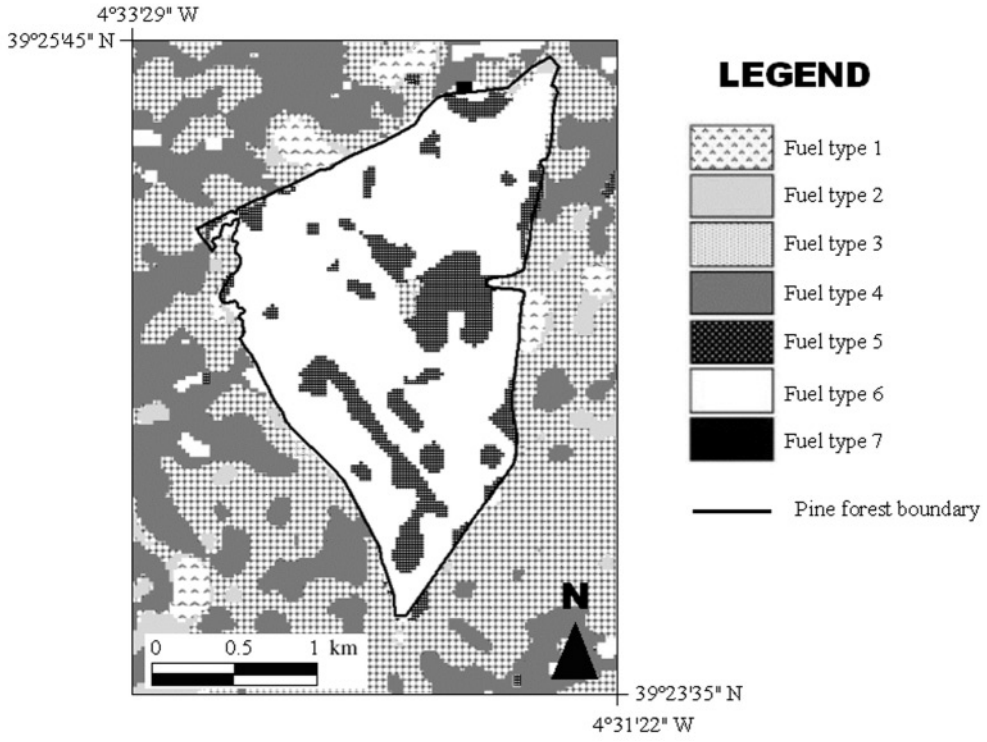

Fig. 10. The boundary of shrub species from the photointerpreted map are superimposed on the fuel type map produced by digital classification.

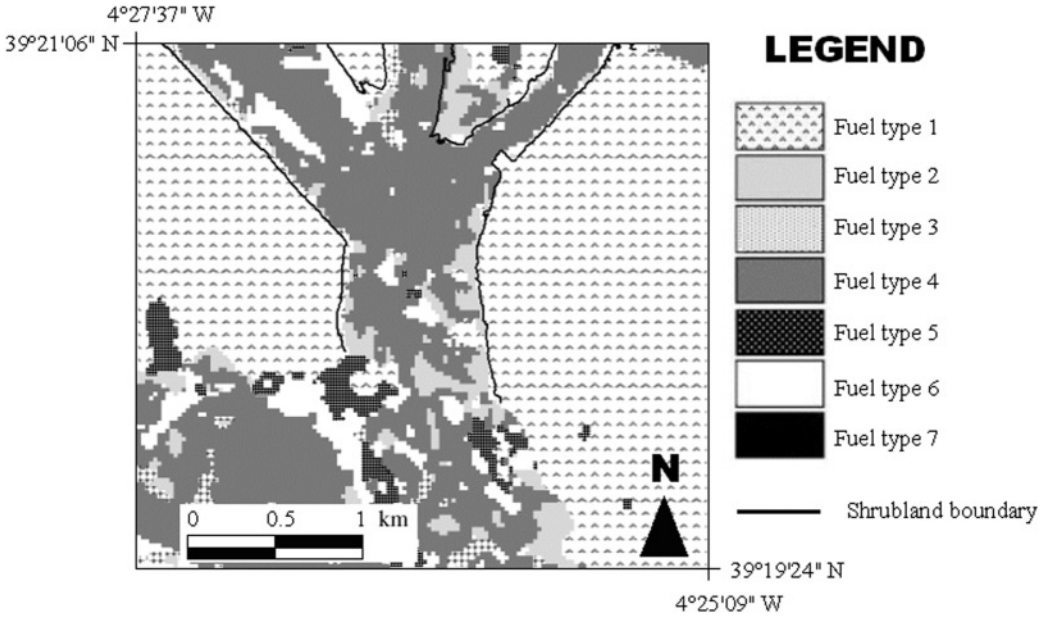

Conclusions

The main conclusions are as follows.

(1) Atmospheric disturbances and topographic shadowing affects the distinction of fuel types. Atmospheric correction produced an improvement in the spectral characterization of the fuel types classes, and topographic correction reduced spectral variability within each class.
(2) The best layers for the classification of fuel types were texture, topographic variables, and TM1–TM6 from both dates (May 5, 1998, and July 24, 1998).
(3) Synthetic variables (vegetation indices, endmembers) were not particularly useful, because the original variables were already involved in the classification. Therefore, to avoid redundant information, neither of them should be used.
(4) Satellite data and ancillary information provide an accurate discrimination of fuel types (global classification accuracy 82.8%).
(5) Remote sensing (Landsat TM) relies on superficial observation of reflectance or temperature from the canopy layer, and therefore, it is difficult to identify the understory component of the forest depth. Additionally, reflectance is not directly related to vegetation height, which is a critical variable to discriminate fuel types. Surface temperature is more related to it, since the pattern of surface temperature depends on the height of the vegetation.
(6) An operational methodology was provided to identify fuel types at regional scale, based on the use of remote sensing (Landsat TM), ancillary layers, and limited fieldwork.

Future research should be directed to avoiding misclassifications by retrieving more direct information on vegetation height. Radar has been tested to obtain canopy height in the Brazilian forests (Toutin and Amaral 2000), but accuracy was only ±5 m. Its vertical accuracy cannot be less than 1 m because of issues underlying microwave reflections (Hill et al. 2000). This is too coarse for fuel types description in Mediterranean ecosystems. In addition, it is difficult to correct topographic distortion in radar data. Other techniques such as LIDAR (active sensors working with laser) should be tested (Blair et al. 1999). This technology will be useful not only for overstory vegetation height estimation but also for the estimating the height of understory vegetation, with accuracy up to ±0.10 m. Spectral characterization of fuel types using a hyperspectral sensor will improve classification results (Ustin and Trabucco 2000). These new technologies should become available at regional scale.

Acknowledgements

This research has been funded by the Control-Fire-Sat (ENV4-CT97-0479) and Inflame projects (ENV4-CT98-0700) under the Environment and Climate Program of the European Commission (DG-XII). The authorities of the Cabañeros National Park helped in the fieldwork and have kindly provided ancillary data. Financial support was also obtained from the Spanish Ministry of Science through project No. AGF96-2094-CE. We acknowledge the Autonomous Region of Madrid, Spain, who financed D.R. for this study. Finally, we thank Robert Burgan who kindly reviewed this paper.

References

Agee, J.K., and Pickford, S.G. 1985. Vegetation and fuel mapping of North Cascades National Park. Final Report. College of Forest Resources, University of Washington, Seattle, Wash.

Albini, F.A. 1976. Estimating wildfire behavior and effects. USDA For. Serv. Gen. Tech. Rep. INT-30.

Anderson, H.E. 1982. Aids to determining fuel models for estimating fire behavior. USDA For. Serv. Gen. Tech. Rep. INT-122.

Andrews, P.L. 1986. BEHAVE: fire behavior prediction and fuel modeling system. Burn subsystem. Part 1. USDA For. Serv. Gen. Tech. Rep. INT-194.

Beaudoin, A., Deshayes, M., Piet, L., Stussi, N., and Le Toan, T. 1994. Retrieval and analysis of temperature forest backscatter signatures from multitemporal ERS-1 data acquired over hilly terrain. *In* First ERS-1 Pilot Project Workshop, Toledo, Spain. European Space Agency, Paris. pp. 283–289.

Blair, J.B., and Hofton, M.A. 1999. Modeling laser altimeter return waveforms over complex vegetation using high-resolution elevation data. Geophys. Res. Lett. **26**: 2509–2512.

Blair, J.B., Rabine, D.L., and Hofton, M.A. 1999. The laser vegetation imaging sensor: a medium-altitude, digitisation-only, airborne laser altimeter for mapping vegetation and topography. ISPRS J. Photogramm. Remote Sens. **54**: 115–122.

Burgan, R.E., and Shasby, M.B. 1984. Mapping broad-area fire potential from digital fuel, terrain, and weather data. J. For. **82**: 228–231.

Castro, R., and Chuvieco, E. 1998. Modeling forest fire danger from geographic information systems. Geocarto Int. **13**: 15–23.

Chavez, P.S. 1996. Image-based atmospheric corrections. Revisited and improved. Photogramm. Eng. Remote Sens. **62**: 1025–1036.

Chuvieco, E., and Salas, F.J. 1996. Mapping the spatial distribution of forest fire danger using GIS. Int. J. Geogr. Inf. Syst. **10**: 333–345.

Congalton, R.G. 1991. A review of assessing the accuracy of classifications of remotely sensed data. Remote Sens. Environ. **37**: 35–46.

Congalton, R.G., and Green, K. 1999. Assessing the accuracy of remotely sensed data: principles and applications. Lewis Publishers, Boca Raton, Fla.

Cosentino, M.J., Woodcock, C.E., and Franklin, J. 1981. Scene analysis for wildland fire — fuel characteristics in a Mediterranean climate. *In* Proceedings, 15th International Symposium on Remote Sensing of Environment, Ann Arbor, Mich. Environmental Research Institute of Michigan, Ann Arbor, Mich. pp. 635–646.

Deeming, J.E., Burgan, R.E., and Cohen, J.D. 1978. The national fire-danger rating system — 1978. USDA For. Serv. Gen. Tech. Rep. INT-39.

De Wulf, R.R., Goossens, R.E., Deroover, B.P., and Borry, F.C. 1990. Extraction of forest stand parameters from panchromatic and multispectral SPOT-1 data. Int. J. Remote Sens. **11**: 1571–1588.

Dikshit, O., and Roy, D.P. 1996. An empirical investigation of image resampling effects upon the spectral and textural supervised classification of a high spatial resolution multispectral image. Photogramm. Eng. Remote Sens. **62**: 1085–1092.

Dixon, R., Shipley, R., and Briggs, A. 1984. Landsat — a tool for mapping fuel types in the boreal forest of Manitoba. A pilot study. Manitoba Remote Sensing Center, Fire Management and Communications Section, Canada Centre for Remote Sensing, Winnipeg, Man.

Fenstermaker, L.K. 1994. Remote sensing thematic accuracy assessment: a compendium. American Society for Photogrammetry and Remote Sensing, Bethesda, Md.

Gilabert, M.A., Conese, C., and Maselli, F. 1994. An atmospheric correction method for the automatic retrieval of surface reflectances from TM images. Int. J. Remote Sens. **15**: 2065–2086.

Haralick, R.M., Shanmugan, K., and Dinstein, I. 1973. Textural features for image classification. IEEE Trans. Syst. Man Cybernetics, **3**: 610–621.

Hill, J.M., Graham, L.A., and Henry, R.J. 2000. Wide-area topographic mapping and applications using airborne light detection and ranging (LIDAR) technology. Photogramm. Eng. Remote Sens. **66**: 908–909, 911–914, 927, 960.

Hunt, E.R., and Rock, B.N. 1989. Detection of changes in leaf water content using near and middle-infrared reflectances. Remote Sens. Environ. **30**: 43–54.

Hyyppa, J., and Hallikainen, M. 1996. Applicability of airborne profiling radar to forest inventory. Remote Sens. Environ. **57**: 39–57.

Hyyppa, J., Hyyppa, H., Inkinen, M., Engdahl, M., Linko, S., and Zhu, Y.H. 2000. Accuracy comparison of various remote sensing data sources in the retrieval of forest stand attributes. For. Ecol. Manage. **128**: 109–120.

Hyyppa, J., Kelle, O., Lehikoinen, M., and Inkinen, M. 2001. A segmentation-based method to retrieve stem volume estimates from 3-D tree height models produced by laser scanners. IEEE Trans. Geosci. Remote Sens. **39**: 969–975.

Khorram, S. 1999. Accuracy assessment of remote sensing-derived change detection. American Society for Photogrammetry and Remote Sensing, Bethesda, Md.

Kourtz, P.H. 1977. An application of Landsat digital technology to forest fire fuel type mapping. *In* Proceedings, 11th International Symposium on Remote Sensing of Environment, Ann Arbor, Mich. Environmental Research Institute of Michigan, Ann Arbor, Mich. pp. 1111–1115.

Kumar, R., and Silva, L.F. 1977. Separability of agricultural cover types by remote sensing in the visible and infrared wavelength regions. IEEE Trans. Geosci. Electron. **15**: 49–59.

Lawson, B.D., Stocks, B.J., Alexander, M.E., and Van Wagner, C.E. 1985. A system for predicting fire in Canadian forests. *In* Proceedings, 8th Conference on Fire and Forest Meteorology, Detroit, Mich. Society of American Foresters, Bethesda, Md.

Lefsky, M.A., Cohen, W.B., and Spies, T.A. 2001. An evaluation of alternate remote sensing products for forest inventory, monitoring, and mapping of Douglas-fir forests in western Oregon. Can. J. For. Res. **31**: 78–87.

McKinley, R.A., Chine, E.P., and Werth, L.F. 1985. Operational fire fuels mapping with NOAA-AVHRR data. *In* Tenth Pecora Memorial Remote Sensing Symposium: Remote Sensing in Forest and Range Resource Management. American Society for Photogrammetry and Remote Sensing, Bethesda, Md. pp. 295–304.

Merrill, D.F., and Alexander, M.E. 1987. Glossary of forest fire management terms. National Research Council of Canada, Committee for Forest Fire Management, Ottawa, Ont.

Meyer, P., Itten, K.I., Kellenbenberger, T., Sandmeier, S., and Sandmeier, R. 1993. Radiometric corrections of topographically induced effects on Landsat TM data in an alpine environment. ISPRS J. Photogramm. Remote Sens. **48**: 17–28.

Oswald, B.P., Fancher, J.T., Kulhavy, D.L., and Reeves, H.C. 1999. Classifying fuels with aerial photography in East Texas. Int. J. Wildland Fire, **9**: 109–113.

PCI. 1999. Using PCI software. PCI, Richmond Hill, Ont.

Roberts, D.A., Green, R.O., and Adams, J.B. 1997. Temporal and spatial patterns in vegetation and atmospheric properties from AVIRIS. Remote Sens. Environ. **62**: 223–240.

Rosenfeld, A., and Pfaltz, J. 1968. Distance functions on digital pictures. Pattern Recog. **1**: 33–61.

Rouse, J.W., Haas, R.W., Schell, J.A., Deering, D.H., and Harlan, J.C. 1974. Monitoring the vernal advancement and retrogradation (Greenwave effect) of natural vegetation. Type III Final Report National Aeronautics and Space Administration, Goddard Space Flight Center, Greenbelt, Md.

Shimabukuro, Y.E., and Smith, J.A. 1991. The least-squares mixing models to generate fraction images derived from remote

sensing multispectral data. IEEE Trans. Geosci. Remote Sens. **29**: 16–20.

Swain, P.H., and Davis, S.M. (*Editors*). 1978. Remote sensing: the quantitative approach. McGraw-Hill, New York.

Toutin, T., and Amaral, S. 2000. Stereo RADARSAT data for canopy height in Brazilian forests. Can. J. Remote Sens. **26**: 189–199.

Ustin, S.L., and Trabucco, A. 2000. Using hyperspectral data to assess forest structure. J. For. **98**: 47–49.

Van Wagtendonk, J.W., and Root, R.R. 2002. The use of multitemporal Landsat normalized difference vegetation index (NDVI) data for mapping fuel models in Yosemite National Park, U.S.A. Int. J. Remote Sens. In press.

Vasconcelos, M.J.P., Paúl, J.C.U., Silva, S., Pereira, J.M.C., Caetano, M.S., Catry, F.X., and Oliveira, T.M. 1998. Regional fuel mapping using a knowledge based system approach. *In* Proceedings, 3rd International Conference on Forest Fire Research — 14th Conference on Fire and Forest Meteorology, Coimbra. *Edited by* D.X. Viegas. University of Coimbra, Coimbra. pp. 2111–2123.

Vélez, R. 2000. La defensa contra incendios forestales. Fundamentos y experiencias. 1st ed. McGraw-Hill/Interamericana de España S.A.U., Madrid.

Wukelic, G.Z., Gibbons, D.E., Martucci, L.M., and Foote, H.P. 1989. Radiometric calibration of Landsat Thematic Mapper thermal band. Remote Sens. Environ. **28**: 339–347.

Yool, S.R., Eckhardt, D.W., Cosentino, M.J., and Estes, J.E. 1984. A geographic information system approach to quantitative assessment of wildlife fuels. *In* Proceedings, ACSM–ASPRS Annual Convention, Washington, D.C. America Society for Photogrammetry and Remote Sensing, Bethesda, Md. pp. 792–801.

Zhu, Z., and Evans, D.L. 1994. U.S. forest types and predicted percent forest cover from AVHRR data. Photogramm. Eng. Remote Sens. **60**: 525–531.